J. Fluid Mech. (2003), *vol.* 487, *pp.* 125–145.
DOI: 10.1017/S0022112003004737 Printed in the United Kingdom

On the convective nature of bar instability

By B. FEDERICI AND G. SEMINARA

Department of Environmental Engineering, University of Genova,
Via Montallegro 1, 16145 Genova, Italy
sem@diam.unige.it

(Received 29 March 2002 and in revised form 9 January 2003)

Bar instability is recognized as the fundamental mechanism underlying the formation of large-scale forms of rivers. We show that the nature of such instability is convective rather than absolute. Such a result is obtained by revisiting the linear stability analysis of open-channel uniform flow over a cohesionless channel of Colombini *et al.* (1987) and using the Briggs (1964) criterion to distinguish between the convectively and absolutely unstable temporally asymptotic response to an initial boundary-value perturbation of bed topography. Examining the branch-point singularities of the dispersion relation, which can be determined in closed form, we show that all the existing branch-point singularities characterized by positive bar growth rate ω_i, involve spatial branches of the dispersion relation which, for large positive values of ω_i, lie in the same half λ-plane, λ denoting the complex bar wavenumber. Hence, the nature of instability is convective and remains so for any value of the aspect ratio, the controlling parameter of the basic instability, as well as for any lateral mode investigated. The latter analytical findings are confirmed by numerical solutions of the fully nonlinear problem. In fact, starting from either a randomly distributed or a localized spatial perturbation of bed topography, groups of bars are found to grow and migrate downstream leaving the source area undisturbed. The actual bars observed in laboratory experiments arise from the spatial-temporal growth of some persistent initial perturbation. The nonlinear development of such perturbations is shown to lead to a periodic pattern with amplitude independent of the amplitude of the initial perturbation. Bars are also found to lengthen and slow down as they grow from the linear into the nonlinear regime, in agreement with experimental observations. The distance from the initial cross-section at which equilibrium is achieved depends on the initial amplitude of the perturbation, a finding which calls for a revisitation of classical laboratory observations reported in the literature.

1. Introduction

Bars are large-scale bedforms which are observed in rivers. Following Seminara & Tubino (1989*a*), it is convenient to distinguish between two classes of bar, respectively called free and forced.

Free bars arise from an instability of the cohesionless bottom of a channel, whereby a small wavy perturbation of bottom elevation grows in time. The outcome of such an instability is the development of alternating sequences of riffles and pools separated by diagonal fronts, which may occur either in single rows (alternate bars, figure 1*a*) or in multiple rows (multiple row bars, figure 1*b*). Each of the units composing such patterns is characterized by a lateral scale equal to an integral fraction of the channel width, a longitudinal scale of the order of a few times (say six times) the

FIGURE 1. (*a*) Alternate bars in a reach of the Elbow river (courtesy of G. Parker); (*b*) multiple bars in the Waimakariri River, New Zealand (pictures taken by B. Federici).

lateral scale, amplitude of the order of the average flow depth and slow downstream migration. An extensive literature on bar formation has grown starting from the seminal work of Callander (1969). It is now fairly well established that the formation of bars can be explained by a classical normal mode stability analysis performed on the system of conservation equations governing the hydrodynamics and sediment transport in channels with a cohesionless bed (e.g. Colombini, Seminara & Tubino 1987). Alternate bars are then described by the first (lateral) Fourier mode while multiple row bars are associated with higher-order lateral modes. The inception of instability is found to be controlled by a delicate balance between the destabilizing contribution associated with the secondary flow and the stabilizing contribution mainly associated with the effect of gravity on sediment transport. The former turns out to be crucially dependent on the longitudinal bar wavenumber, the latter increases as the lateral slope of the bed increases. Hence, a given small-amplitude bottom perturbation is increasingly stabilized as the aspect ratio of the channel β decreases; in other words, very narrow channels do not allow for bar formation, fairly narrow channels display the development of alternate bars while very wide channels lead to the formation of multiple row bars. The aspect ratio of the channel is the crucial dimensionless parameter for the instability. However, some weaker role is also played by the Shields parameter τ_*, a dimensionless form of the average bottom stress (see equation (2.1)) which is known to control the intensity of sediment transport, and by the relative roughness parameter d_s which controls frictional forces. For given Shields stress and relative roughness, linear stability (e.g. Colombini *et al.* 1987) predicts a sequence of increasing critical values β_{cm} above which small-amplitude bar perturbations characterized by m rows are amplified. For $m = 1$, bars give rise to a weakly meandering pattern of the thalweg, whereas for $m \geqslant 2$, a submerged

braiding pattern develops. For this reason, it has long been speculated (Leopold & Wolman 1957) that alternate bars would be precursors of meanders, while multiple row bars would ultimately develop into a braided river.

Forced bars arise from forcing effects, typically channel curvature, variations of channel width or non-uniform initial conditions. In particular, in a meandering channel, the periodic variation of channel curvature drives a secondary flow which leads to the establishment of a periodic sequence of regions of depositions at the inner bends and scours at the outer bends which have a structure similar to that of alternate bars except for their non-migrating character. Forced bars have also been intensely investigated, in particular in the context of theories of meander formation (Ikeda & Parker 1989). In particular, the bend theory of river meanders (Ikeda, Parker & Sawai 1981; Blondeaux & Seminara 1985), suggests that planimetric perturbations of the channel axis characterized by wavenumbers smaller than some threshold value do amplify, leading to meander growth. The speculation of Leopold & Wolman (1957), namely the interpretation of alternate bars as precursors of meanders, would then require that planimetric perturbations of the channel axis with wavenumber equal to that of alternate bars should indeed be found to be planimetrically unstable. Unfortunately, this is not the case as the bar wavenumber typically exceeds the threshold value of meander wavenumber above which planimetric perturbations are found to be damped; such a finding seems to contradict the idea that alternate bars are indeed precursors of meanders.

However, laboratory observations (Federici 1999; Federici & Paola 2003) of the development of river patterns starting from a straight channel initially cut in a uniform cohesionless floodplain (figure 2*a*) do point at the important role that the initial formation of alternate bars may play. They appear to trigger small periodic width variations of the channel (figure 2*b*) which stop bar migration and then lead to bank erosion and channel meandering (figure 2*c*), though the subsequent development of the pattern in a cohesionless environment where bank erosion occurs on the same time scale of bottom erosion, invariably leads eventually to a braided configuration (figure 2*d*).

A deeper understanding of the nature of the process of free bar formation is then called for in order to make further progress in the understanding of river meandering and river braiding.

A striking feature of the bar-meandering patterns, typically observed in laboratory investigations of the type performed by Federici (1999), is the spatial propagation of the observed feature. This observation points to the need to ascertain the nature of the bar instability mechanism. In fact, it is well known that instability is described as convective provided an initial small perturbation localized in space is convected downstream leaving, as time tends to infinity, the flow domain unperturbed. On the contrary, instability is described as absolute whenever the initial small localized perturbation spreads both in the upstream and downstream directions as time grows, affecting eventually the whole flow domain. Such a fundamental distinction was originally proposed in the field of plasma physics by Briggs (1964) and Bers (1975, 1983) and has since been applied and developed in hydrodynamic stability by several authors (see the review of Huerre & Monkewitz 1990). Temporal stability analyses of bar formation of the kind performed by most investigators (e.g. Callander 1969; Engelund & Skovgaard 1973; Colombini *et al.* 1987, hereinafter referred to as CST) consider perturbations which amplify in time, starting from some initial spatially periodic perturbation, i.e. they assume that the perturbation wavenumber λ is real while its frequency ω is complex. Such analyses allow us to distinguish between stable

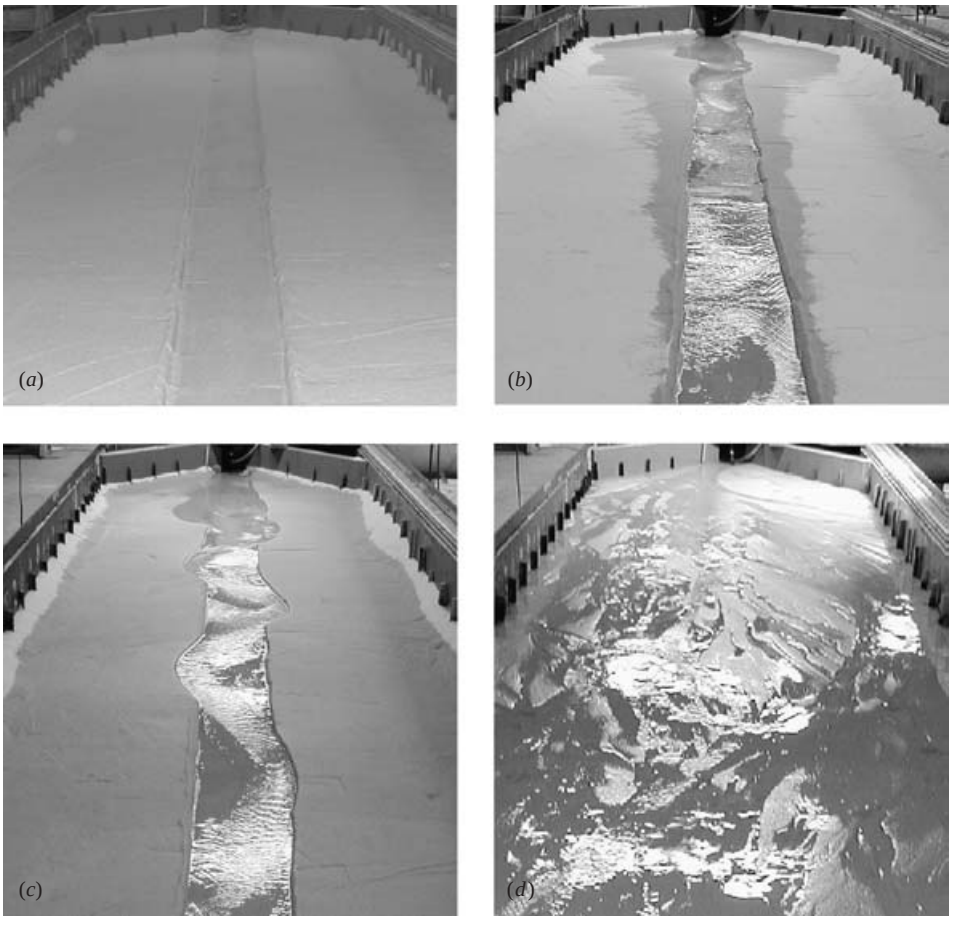

FIGURE 2. Laboratory observations of the development of river patterns: (*a*) $t = 0$: a straight channel is initially cut in a cohesionless floodplain; (*b*) $t = 5$ min: alternate bars form; (*c*) $t = 20$ min: small periodic width variations of the channel, triggered by the alternate bars, stop bar migration and lead to bank erosion and channel meandering; (*d*) $t = 20$ h: a braided pattern.

configurations (all λ decay in time) and unstable systems (some λ are amplified). When the nature of the instability is convective a spatial stability analysis is applicable, considering perturbations which evolve in space, starting from some initial temporal distribution, i.e. assuming that the perturbation wavenumber is complex and the perturbation frequency is real.

In order to ascertain the nature of the instability, the response of the system to impulsive forcing must be investigated. As first discussed by Briggs (1964), absolute instability is associated with the occurrence of branch-point singularities in the dispersion relationship, i.e. values of ω and λ (both complex) where two or more spatial branches of the dispersion relationship merge (a spatial branch being defined as the locus of solutions of the dispersion relationship associated with any given value of the imaginary part of ω, in the following denoted by ω_i). Branch-point singularities (ω_o, λ_o) are characterized by vanishing values of the longitudinal group velocity $[\partial\omega/\partial\lambda]_{\omega_o,\lambda_o}$. More precisely, in order for the instability to be absolute, the perturbation growth rate ω_i at the branch point must be positive; furthermore, as we move from

the singularity, increasing the value of ω_i, at least two of the spatial branches of the dispersion relationship that merge in the singularity must lie in distinct half λ-planes for sufficiently large values of ω_i.

Applying such a criterion to the case of bar instability is fairly straightforward as the dispersion relationship is derived in closed form for any given transverse Fourier mode m, identifying the number of rows characterizing the bar perturbation. As discussed in the paper, it turns out that, at a linear level, bar instability is invariably convective.

Such findings can be substantiated at a nonlinear level by performing numerical simulations on the fully nonlinear equations governing the morphodynamical problem. More precisely, the response of flow and bed topography to either randomly distributed or localized spatial initial perturbations is shown to give rise to the growth of wave groups which migrate downstream leaving the flow domain unperturbed.

The rest of the paper will proceed as follows. In the next section, we briefly recall the mathematical formulation of the problem of morphodynamics. In § 3, we summarize the classical results of linear stability of uniform flow and bed topography in straight cohesionless channels and prove the convective nature of the instability based on the properties of branch singularities of the dispersion relationship. Section 4 is devoted to describe some numerical simulations of the fully nonlinear problem which substantiate the theoretical findings. Having ascertained the convective nature of the instability, some questions concerning the properties of the spatial development of free bars arise. In § 5, we provide some answers to them through the results of a series of suitable numerical experiments. Finally, some concluding remarks complete the paper.

2. Formulation of the problem

The mechanical system under investigation is an incompressible fluid, flowing in a wide open channel with an erodible cohesionless bottom and non-erodible banks. Flow is turbulent and sufficiently intense to entrain sediments through the bed interface. Hence, having defined the dimensionless Shields stress τ_* (denoted by θ in CST) in the form:

$$\tau_* = \frac{u_\tau^2}{(s-1)gd}, \tag{2.1}$$

with u_τ the local value of the friction velocity, s the relative density of sediments, g the acceleration due to gravity and d the uniform grain size, we assume that τ_* exceeds everywhere its critical value τ_{*c} associated with the threshold of motion. In fact, it is well established since the early work of Shields (1936) that the entrainment of sediment particles lying on a cohesionless bed statistically vanishes for values of τ_* smaller than τ_{*c}, a quantity found to depend on the particle Reynolds number R_p, defined as:

$$R_p = \frac{\sqrt{(s-1)gd^3}}{\nu}. \tag{2.2}$$

We also assume that Shields stress does not exceed a second threshold value $\tau_{*s}(R_p)$, below which particle motion occurs in the form of saltation (or through rolling and sliding) within a layer close to the bed interface of typical thickness of the order of $2d$–$3d$. Such a mode of transport is called bedload; under these conditions particles are not entrained in suspension, i.e. their motion does not extend to the bulk of the flow. Such restriction allows for a simpler treatment of the stability problem,

but is by no means essential and could be readily removed (see for instance Repetto Tubino & Zolezzi 1999; Seminara & Tubino 2001). The problem of bar formation can then be formulated taking advantage of the fact that bars have typical wavelengths of the order of a few channel widths, a feature which suggests that we can safely employ the shallow-water equations to describe the hydrodynamics except, possibly, close to the relatively sharp oblique bar fronts which develop in the finite-amplitude regime. Recalling that the evolution of the bed interface resulting from the continuous process of entrainment and distrainment of bedload particles is governed by the two-dimensional form of Exner's (1925) equation, we end up with the following differential problem (CST):

$$\epsilon U_{,t} + UU_{,s} + VU_{,n} + H_{,s} + \beta\frac{\tau_s}{D} = 0, \tag{2.3a}$$

$$\epsilon V_{,t} + UV_{,s} + VV_{,n} + H_{,n} + \beta\frac{\tau_n}{D} = 0, \tag{2.3b}$$

$$\epsilon D_{,t} + (UD)_{,s} + (VD)_{,n} = 0, \tag{2.3c}$$

$$\left(F_o^2 H - D\right)_{,t} + Q_{s,s} + Q_{n,n} = 0. \tag{2.3d}$$

In (2.3*a*)–(2.3*d*) we have employed the following notations: s and n are longitudinal and lateral Cartesian coordinates, respectively, with s aligned with channel axis; U and V are longitudinal and lateral components of the depth-averaged velocity, respectively; H and D are free-surface elevation and flow depth, respectively; τ_s and τ_n are longitudinal and lateral components of the bottom stress, respectively; Q_s and Q_n are longitudinal and lateral components of the depth averaged sediment flux, respectively; t is time. Note that dimensional quantities (denoted below by a circumflex) have been made dimensionless employing the following scales:

$$(s, n) = (\hat{s}, \hat{n})/B, \qquad (U, V) = (\hat{U}, \hat{V})/U_o, \tag{2.4a}$$

$$\left(F_o^2 H, D\right) = (\hat{H}, \hat{D})/D_o, \qquad t = \hat{t}/[B/(\epsilon U_o)], \tag{2.4b}$$

$$(\tau_s, \tau_n) = (\hat{\tau}_s, \hat{\tau}_n)/\rho U_o^2, \qquad (Q_s, Q_n) = (\hat{Q}_s, \hat{Q}_n)/\sqrt{(s-1)gd^3} \tag{2.4c}$$

where B is the half-width of the channel, U_o and D_o are average flow speed and flow depth associated with the uniform flow of the given flow discharge in a channel with the given constant slope S, while ϵ is the small ratio between the hydrodynamic and morphodynamic time scales, which reads:

$$\epsilon = \frac{\sqrt{(s-1)gd^3}}{(1-p)D_o U_o}. \tag{2.5}$$

Here, p is porosity of the granular medium, a quantity which is typically about 0.4, and s is the ratio between sediment and water density. Note that the parameter ϵ coincides with the Q_o parameter defined by (6*a*) of CST. It attains values ranging typically about 10^{-3}–10^{-4}, hence we can safely ignore unsteady effects driven by the bed evolution in the hydrodynamic equations.

Finally, two dimensionless parameters arise, namely the aspect ratio β and the Froude number F_o of the uniform reference flow, which read:

$$\beta = \frac{B}{D_o}, \qquad F_o^2 = \frac{U_o^2}{gD_o}. \tag{2.6}$$

Note that the aspect ratio β is the main controlling parameter of bar instability.

Progress with the above formulation requires that the governing equations (2.3*a*)–(2.3*d*) be supplemented with closure relationships for bottom stress and sediment flux.

Following the classical closure also employed in CST, we write:

$$\boldsymbol{\tau} = (\tau_s, \tau_n) = C(U, V)\sqrt{U^2 + V^2}, \tag{2.7}$$

with C the friction coefficient which, for the case of a plane undisturbed bed, may be given the classical logarithmic form:

$$C = \left[6 + 2.5 \ln\left(\frac{D}{2.5d_s}\right)\right]^{-2}, \tag{2.8}$$

where d_s is the relative roughness (d/D_o). Essentially, using the latter scheme we are modelling frictional effects as driven by a slowly varying sequence of locally and instantaneously uniform flows, an assumption justified by the spatial scale of bars largely exceeding the local flow depths and by the extremely slow temporal development of bars measured by the small parameter ϵ (see equation (2.5)).

Closure for the bedload flux requires the provision of relationships able to quantify both intensity and direction of sediment transport. For uniform plane turbulent flows on cohesionless beds, it is fairly well established that the average bedload motion is aligned with the average flow and its intensity is a monotonically increasing function of the excess Shields stress $\Phi(\tau_* - \tau_{*c})$, for which various empirical relationships have been proposed in the literature. Under the latter conditions we may then write:

$$\boldsymbol{Q} = (Q_s, Q_n) = (1, 0)\Phi(\tau_* - \tau_{*c}). \tag{2.9}$$

Below we will employ for Φ the classical Meyer-Peter & Müller (1948) form:

$$\Phi = 8(\tau_* - \tau_{*c})^{3/2}. \tag{2.10}$$

Moreover, in order to check that the results of the present analysis are not significantly dependent on the particular form chosen for the closure relationship for Φ, we have repeated our calculations replacing (2.10) by Parker's (1990) relationship:

$$\phi = 0.00218\tau_*^{3/2}G(\xi), \qquad \xi = \tau_*/\tau_{*rif}, \qquad \tau_{*rif} = 0.0386, \tag{2.11}$$

where:

$$G = 5474(1 - 0.853/\xi)^{4.5}, \qquad \xi \geqslant 1.59, \tag{2.12a}$$

$$G = \exp[14.2(\xi - 1) - 9.28(\xi - 1)^2], \qquad 1 \leqslant \xi \leqslant 1.59, \tag{2.12b}$$

$$G = \xi^{14.2}, \qquad \xi \leqslant 1, \tag{2.12c}$$

which is known to perform well for gravel bed rivers.

However, a crucial feature of bars is the sloping character of their bed. When attempting to extend (2.9) to configurations characterized by non-negligible values of the local bed slope, we have to account for the physical fact that, under such conditions, sediment motion tends to deviate from the local direction of the mean flow, to accomplish the gravitational tendency of particles to move preferentially downhill. Such an effect has been investigated thoroughly in the last two decades. Assuming the bed to be 'weakly' sloping, an assumption appropriate to describe bars, except perhaps close to their 'sharp' diagonal fronts, we may write:

$$\boldsymbol{Q} = (Q_s, Q_n) = (\cos\gamma, \sin\gamma)\Phi. \tag{2.13}$$

Here, γ is the angle that the direction of the bedload flux forms with the longitudinal direction. In the absence of gravitational effects, the average particle motion would be aligned with the average bottom stress, hence $\sin\gamma$ would take the value $V/\sqrt{U^2+V^2}$. A weak lateral local slope of the bed ($\partial\eta^*/\partial n^*$) (with $\eta^* \equiv H^* - D^*$) modifies the latter value, adding a linear contribution to $\sin\gamma$, which can be estimated on the basis of semi-empirical models of particle saltation on weakly sloping beds (Sekine & Parker 1992) or experimental observations (Talmon, Struiksma & Van Mierlo 1995). The outcome of such contributions is the following relationship:

$$\sin\gamma = \frac{V}{\sqrt{U^2+V^2}} - \frac{r}{\beta\sqrt{\tau_*}}\left(F_o^2 H - D\right)_{,n}, \tag{2.14}$$

with r the empirical parameter ranging about 0.5–0.6.

The differential system (2.3a)–(2.3d) with the closure relationships (2.7)–(2.10) must be solved subject to boundary conditions of vanishing fluid and sediment fluxes through the side walls, hence:

$$V = Q_n = 0 \qquad (n = \pm 1), \tag{2.15}$$

as well as to initial conditions to be discussed fully in the next sections.

3. The nature of bar instability

Let us now examine the stability of the basic state consisting of a uniform flow over a plane sloping bed, such that:

$$(U, V, H, D) = (1, 0, H_o, 1). \tag{3.1}$$

We then perturb such a basic state by linear infinitesimal perturbations (u, v, h, d), substitute the perturbed state into the governing differential system with associated closure relationships and boundary conditions and linearize the problem which can eventually be reduced to the following form:

$$\left(\frac{\partial}{\partial t}\mathrm{L} - \mathrm{NM}\right) v = 0, \tag{3.2a}$$

$$v = \frac{\partial^2}{\partial n^2}\left(\frac{\partial}{\partial s} + a_1\right) v = 0 \qquad (n = \pm 1), \tag{3.2b}$$

having denoted by L, N and M the following operators:

$$\mathrm{L} = -\frac{\partial^3}{\partial s^3} - \left[\frac{F_o^2(a_2 - a_1 - a_3) + a_3}{1 - F_o^2}\right]\frac{\partial^2}{\partial s^2} - \left[\frac{1}{1 - F_o^2}\right]\frac{\partial^3}{\partial s \partial n^2} - \left[a_3\frac{F_o^2(a_2 - a_1)}{1 - F_o^2}\right]\frac{\partial}{\partial s} - \left[\frac{a_1}{1 - F_o^2}\right]\frac{\partial^2}{\partial n^2}, \tag{3.3a}$$

$$\mathrm{N} = \frac{(a_5 - a_4)\epsilon\Phi_o}{1 - F_o^2}, \tag{3.3b}$$

$$\mathrm{M} = -\frac{\partial^4}{\partial s^4} + \left[-a_3 - \frac{a_6(1-F_o^2)}{(a_5-a_4)}\frac{\partial^2}{\partial n^2}\right]\frac{\partial^3}{\partial s^3} + \left\{\frac{a_6\left[F_o^2(-a_2+a_1+a_3)-a_3\right]+1-a_5}{(a_5-a_4)}\right\} \times \frac{\partial^4}{\partial s^2 \partial n^2} + \left[\frac{a_6 F_o^2(-a_2+a_1)a_3 + a_1(1-a_5)+a_2(a_4-1)}{(a_5-a_4)} - \frac{a_6}{(a_5-a_4)}\frac{\partial^2}{\partial n^2}\right] \times \frac{\partial^3}{\partial s \partial n^2} - \left[\frac{a_1 a_6}{(a_5-a_4)}\right]\frac{\partial^4}{\partial n^4}, \tag{3.3c}$$

where a_i ($i = 1$–6) are the following coefficients:

$$a_1 = 2\beta C_o, \qquad a_2 = \beta C_o\left(\frac{1}{C_o}\frac{\partial C}{\partial D} - 1\right), \qquad a_3 = \beta C_o, \tag{3.4a}$$

$$a_4 = 2\frac{\tau_{*o}}{\Phi_o}\frac{\partial \Phi}{\partial \tau_*}, \qquad a_5 = \frac{1}{C_o}\frac{\partial C}{\partial D}\frac{\tau_{*o}}{\Phi_o}\frac{\partial \Phi}{\partial \tau_*}, \qquad a_6 = \frac{r}{\beta\sqrt{\tau_*}}, \tag{3.4b}$$

with C_o, τ_{*o} and Φ_o, respectively, denoting the friction coefficient, the Shields stress and the dimensionless bedload transport rate of the undisturbed uniform flow.

The convective or absolute nature of the instability can be ascertained by investigating the impulse response of the system. In other words, we seek the solution of the initial-value problem posed by the differential system (3.2) with initial condition:

$$v = \delta(t)\delta(s)\sum_{m=0}^{\infty}\left\{g_m \cos\left[\tfrac{1}{2}\pi(2m+1)n\right] + h_m \sin(2\pi m n)\right\}, \tag{3.5}$$

where we have denoted by δ a Dirac distribution. Note that each of the lateral modes of the impulse function (3.5) contains Fourier components of all temporal frequencies and longitudinal wavenumbers. In order to analyse the impulse response of the system to (3.5) in a linear context, it is then necessary to determine the structure of the response of the system to each Fourier mode defined as follows:

$$v = g_m \cos\left(\tfrac{1}{2}\pi m n\right)\exp[\mathrm{i}(\lambda s - \omega t)] \qquad (m \text{ odd}), \tag{3.6a}$$

$$v = h_m \sin(\pi m n)\exp[\mathrm{i}(\lambda s - \omega t)] \qquad (m \text{ even}), \tag{3.6b}$$

where λ and ω are complex wavenumber and complex frequency, respectively.

Substituting from (3.6) into the differential problem (3.2), we readily derive the following dispersion relation:

$$D_m(\omega, \lambda; \beta, \tau_*, d_s) = \omega - N\frac{-\lambda^4 + \mathrm{i}n_3\lambda^3 + n_2\lambda^2 + \mathrm{i}n_1\lambda + n_0}{\lambda^3 + \mathrm{i}d_2\lambda^2 + d_1\lambda + \mathrm{i}d_0} = 0. \tag{3.7}$$

The coefficients n_i ($i = 0$–3), d_i ($i = 0$–2) are obtained from the operators (3.3) replacing $\partial/\partial s$ by $(i\lambda)$ and $\partial^j/\partial n^j$ by $(-1)^{e(j)}(\pi m/2)^j$ with $e(j)$ equal to $(j+1)/2$ (or $j/2$) if j is odd (or even) for odd modes, (or equal to $(j-1)/2$ (or $j/2$) if j is odd (or even) for even modes).

The response to the impulse function (3.5) takes the form of a wave packet in the (s, t)-plane. Using the method of steepest descent, we can readily show that, along each ray s/t, the asymptotic behaviour of the response for large times is dominated by the complex wavenumber λ^* such that the associated group velocity is real and satisfies the relationship:

$$\left[\frac{\partial \omega}{\partial \lambda}\right]_{\lambda^*} = \frac{s}{t}. \tag{3.8}$$

The temporal growth rate along the ray s/t is then the growth rate associated with the wavenumber λ^*, namely $(\omega_i(\lambda^*) - (s/t)\lambda_i^*)$. Linear instability occurs if the maximum attainable value over all rays of such growth rate is positive and it is readily shown that the maximum growth rate is experienced by the ray $s/t = [\partial\omega_r/\partial\lambda]_{\lambda_{max}}$ where λ_{max} is the real wavenumber at which the temporal growth rate ω_i of the generic Fourier mode reaches a maximum.

In order to distinguish between convective and absolute instability we must examine the long-term behaviour of the impulse response along the ray $s/t = 0$ at a fixed spatial location. From (3.8), it follows that such behaviour is determined by the growth rate of the complex wavenumber λ_o characterized by vanishing group velocity, i.e. at the branch point of the dispersion relation where:

$$\left[\frac{\partial\omega}{\partial\lambda}\right]_{\lambda_o} = 0. \tag{3.9}$$

Absolute instability requires that $\omega_i(\lambda_o)$ is positive. However, as pointed out by Briggs (1964) and Bers (1975) (see also the review of Huerre & Monkewitz 1990), the latter condition is not sufficient to ensure the absolute character of the instability; the behaviour of the spatial branches of the dispersion relation as we move from the branch point must also be monitored. More precisely, in order for the instability to be absolute, at least two of the spatial branches emerging from the branching point must lie on distinct half λ-planes as ω_i attains large values.

We have applied such a criterion to our stability problem which has the advantage of allowing for the derivation of the dispersion relation in closed form. Hence, we can readily determine the location of the branch-point singularities λ_o as solutions of a complex polynomial of sixth order. Such solutions have been obtained numerically and turned out to be four purely imaginary, and two complex for $\beta_m > \beta_{cm}$, where m is the lateral mode considered. Note that for $\beta_m < \beta_{cm}$, any initial instability with lateral Fourier mode m decays, and so in this case the location of the branch-point singularities is irrelevant. Out of the six solutions, only one purely imaginary (λ_1) and the two complex solutions (λ_2 and $-\bar{\lambda}_2$) are possible candidates for absolute instability, being characterized by a positive value of the growth rate. Such behaviour is displayed for any lateral mode and for any value of the controlling dimensionless parameters. Figure 3 shows the dependence of λ_o and of $\omega(\lambda_o)$ on β for the three solutions of the polynomial of sixth order characterized by positive value of the growth rate, and for the first three lateral modes, given values of Shields stress and relative roughness.

Figures 4 and 5 show how the spatial branches of the dispersion relation behave as we move from every branch-point singularity λ_o characterized by $\omega_i > 0$, with ω_i increasing starting from $\omega_i(\lambda_o)$. It turns out that the two spatial branches emerging from all the branching points invariably lie on the same half λ-plane as ω_i attains sufficiently large values. Hence, at a linear level instability is invariably convective.

Finally, we have checked that our conclusion about the convective nature of bar instability does not depend on the closure relationship for bedload transport. As mentioned in § 2, we have employed Parker's (1990) relationship (equation (2.11)).

The solutions of the complex polynomial of sixth order turn out to be four complex and two purely imaginary for $\beta_m > \beta_{cm}$. Out of the six solutions, only two complex solutions are now possible candidates for absolute instability being characterized by positive value of the growth rate. However, as found above, the two spatial branches of the dispersion relation emerging from the two complex branching points characterized

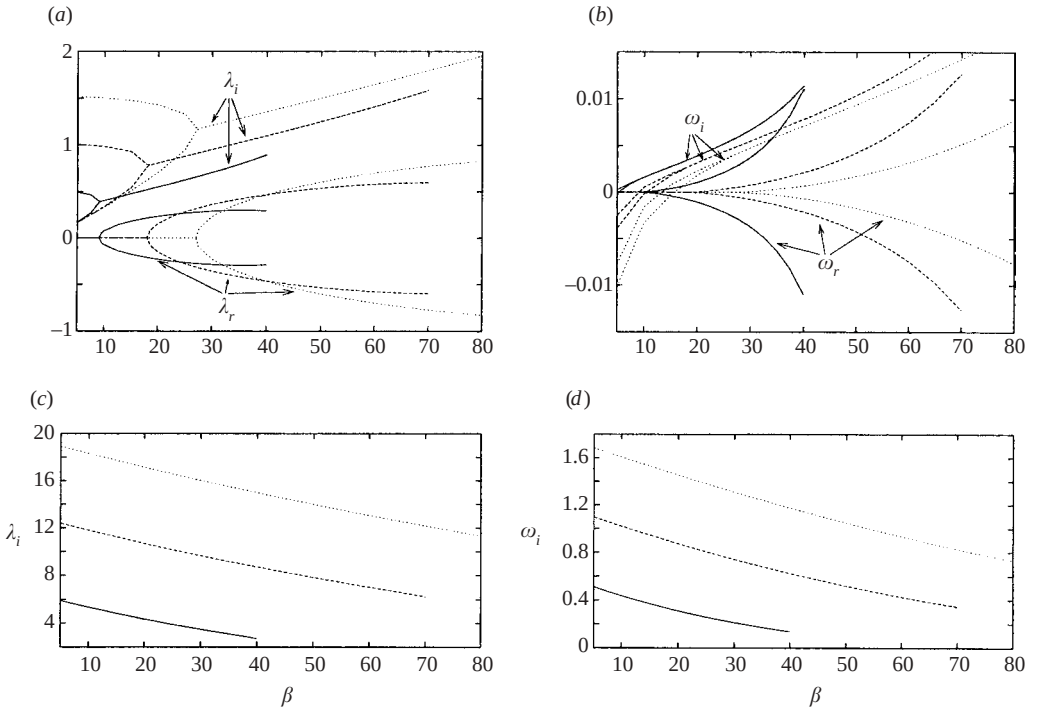

FIGURE 3. Locus of the branch point $(\lambda_o,\omega(\lambda_o))$ as β varies, for $\tau_* = 0.09$, $d_s = 0.04$, and lateral mode $m = 1$ (—), $m = 2$ (- - -), $m = 3$ (. . .); (*a*) and (*b*) are relative to the two complex solutions, (*c*) and (*d*) are relative to the only purely imaginary solution characterized by positive value of the growth rate.

by positive ω_i, invariably lie on the same half λ-plane as ω_i attains sufficiently large values. Hence, our conclusion 'instability is invariably convective' does not seem to depend on the closure relationship for bedload transport used.

In the next section we perform numerical solutions of the fully nonlinear problem to confirm the present analytical findings and to show that the above convective behaviour persists as perturbations evolve into the finite-amplitude regime.

4. Numerical simulations

To perform numerical simulations on the fully nonlinear equations governing the morphodynamical problem, a two-dimensional finite-difference model was built.

We semi-coupled the Exner equation, (2.3*d*), with the shallow-water equations, (2.3*a–c*), and used, for the progress in time, an explicit method for the former and an alternating direction implicit (ADI) method for the latter. The ADI method was chosen to alleviate the problem of a limiting time step for stability reasons, even though, in practice, accuracy requirements will often limit the time step to only a few times the limiting time step for an explicit method. We also added to the equations (2.3*a*, *b*) a diffusive term, namely $\nu\nabla^2(U, V)$ with $\nu = 0.01$, that has merely numerical justification, aimed to improve the stability of the calculation. Moreover, an efficient choice of the location of the variables U, V, H and Z_f $(= F_o^2 H - D)$ on a staggered computational grid was used, as shown in figure 6.

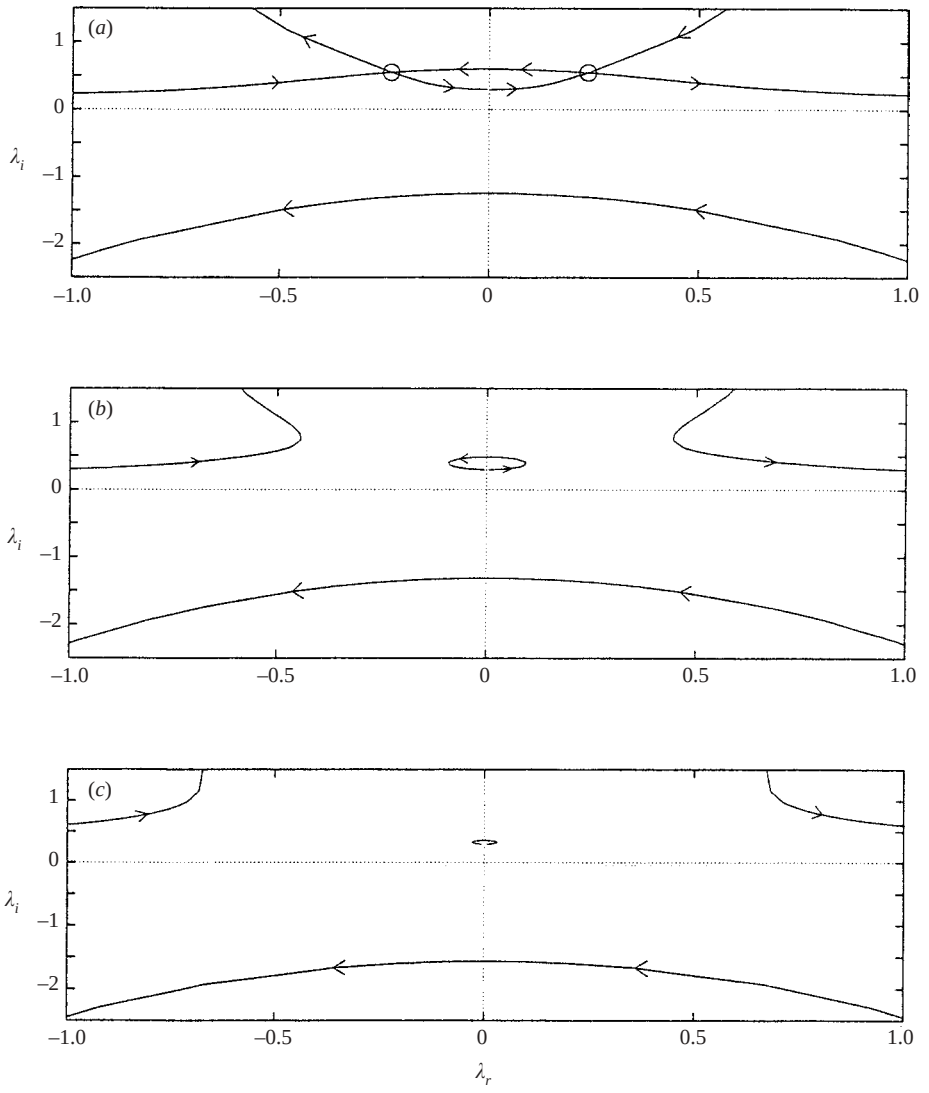

FIGURE 4. The behaviour of the four spatial branches in the λ-plane for the first lateral mode, $\beta = 20$, $\tau_* = 0.09$, $d_s = 0.04$, and (*a*) $\omega_i = \omega_i(\lambda_2) = \omega_i(-\bar{\lambda}_2) \simeq 0.0039$, (*b*) $\omega_i = 0.005$, (*c*) $\omega_i = 0.01$. The two branch-point singularities are marked by a circle. The arrows on the spatial branches indicate the direction of increasing ω_r.

The integrations were performed in two distinct steps. In the first step, we computed the new velocity component U and the new water levels H at time step $k + 1/2$ from information available at time step k and time step $k - 1/2$ using the longitudinal component of the momentum equation and the continuity equation. In the second step, the new velocity component V and the new water levels H at time step $k + 1$ were computed from information available at time step $k + 1/2$ and time step k using the transversal component of the momentum equation and the continuity equation. Note that U was computed only at half-integer time steps, whereas V was computed at integer time steps, and the water level H was computed every half time step. Moreover, we updated the bed topography Z_f every half time step.

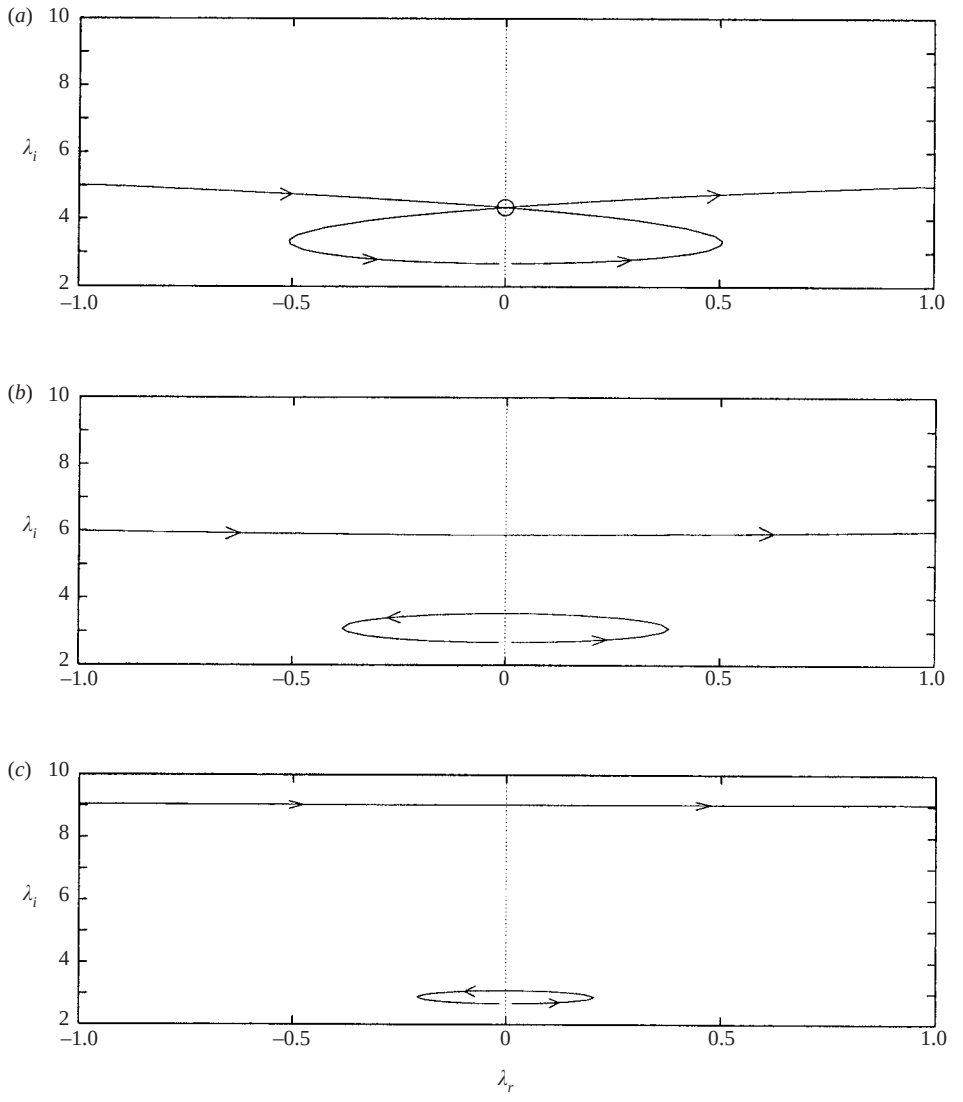

FIGURE 5. The behaviour of the two spatial branches that merge in the purely imaginary branch-point singularity, in the λ-plane for the first lateral mode, $\beta = 20$, $\tau_* = 0.09$, $d_s = 0.04$, and (*a*) $\omega_i = \omega_i(\lambda_1) \simeq 0.311$, (*b*) $\omega_i = 0.350$, (*c*) $\omega_i = 0.500$. The branch-point singularity is marked by a circle. The arrows on the spatial branches indicate the direction of increasing ω_r.

The following boundary conditions were imposed: along the rigid boundaries we set the velocity component V and the lateral sediment flux Q_n equal to zero, the slip condition (no stress) on the velocity U and the water level H horizontal; along the open inflow boundary we set a given water discharge, the longitudinal derivative of V and H to vanish, and constant flow depth, i.e. sediment discharge in equilibrium with the imposed water discharge; finally, along the open outflow boundary we simply set the longitudinal derivative of U, V, H and (Q_s,Q_n) to vanish.

We performed numerical simulations with two different initial conditions: in the first case, we started from a localized spatial perturbation of bed topography, namely a bump with an emisymmetric lateral profile and a sinusoidal longitudinal structure;

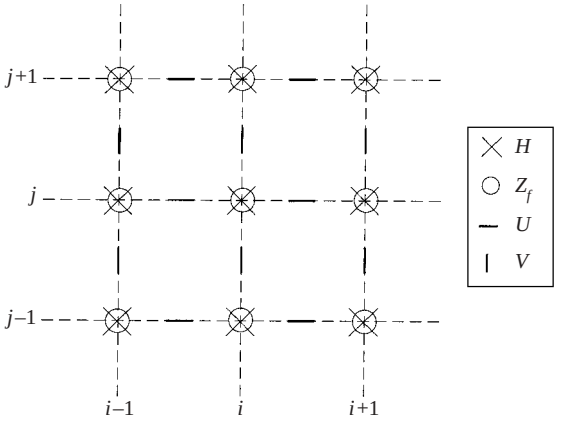

FIGURE 6. Location of U, V, H and Z_f on the difference computational grid.

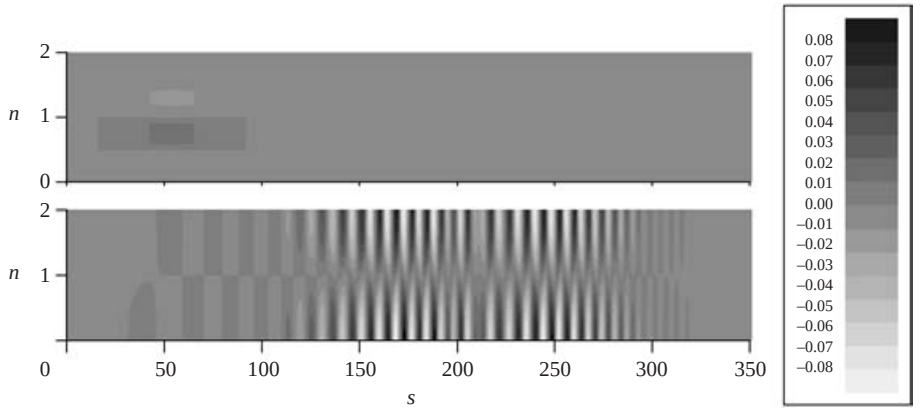

FIGURE 7. Bed topography at the initial time and at $t = 500$ ($\beta = 15$, $\tau_* = 0.09$, $d_s = 0.04$). The initial localized bump gives rise to wave groups that grow and migrate downstream with time.

in the second case, we started from a randomly distributed perturbation of bed topography.

Both the initial conditions gave rise to the growth of wave groups which migrated downstream leaving the flow domain unperturbed, for every aspect ratio of the channel, as shown in figures 7 and 8 (where the darker zone corresponds to deposition and the lighter zone corresponds to erosion). Note that in these figures the lateral scale is much smaller than the longitudinal scale; a three-dimensional view of the actual bed topography is shown in figure 9.

Hence, instability appears to be invariably convective also at a nonlinear level.

5. Discussion

The above results suggest that it is necessary to revisit the interpretation of experimental observations concerning the formation and development of free bars in the laboratory. In fact, the convective nature of the instability mechanism implies that the bars actually observed in the laboratory arise from some forcing effect, e.g.

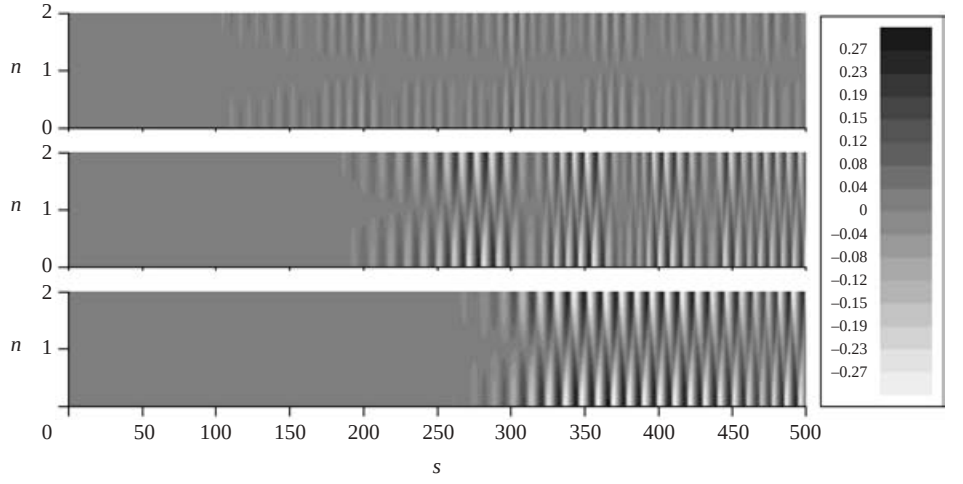

FIGURE 8. Bed topography at $t = 500$, 1000 and 1500 generated by an initial infinitesimal randomly distributed perturbation ($\beta = 12$, $\tau_* = 0.09$, $d_s = 0.04$).

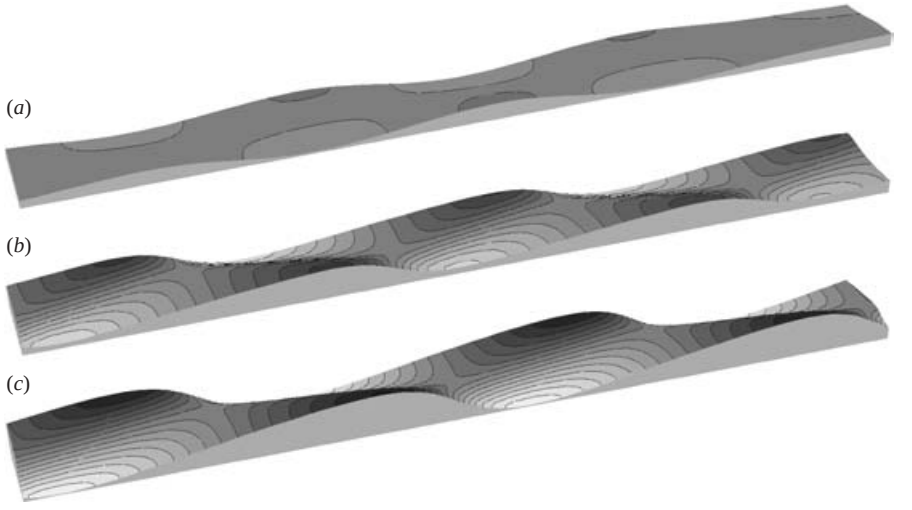

FIGURE 9. Tridimensional view of the bed topography in the random case, close to $s = 400$, at (*a*) $t = 500$, (*b*) 1000 and (*c*) 1500.

a persistent, however small, perturbation of flow and bed topography at the initial cross-section of the channel. Various questions then arise.

Does the forced development of bars eventually lead to the establishment of an equilibrium amplitude of the kind discussed by Colombini et al. (1987)? Is such an equilibrium amplitude dependent on the amplitude of the forced perturbations at the initial cross-section? Does the spatial development require a sufficient length of the laboratory channel? Moreover, how does the selection of the bar mode depend on the spatial rather than temporal character of bar development?

Answering these questions may be pursued through a series of suitable numerical experiments.

Our first numerical experiment, denoted '1Freq', was performed by forcing a persistent perturbation of bottom elevation at the initial cross-section of the flow

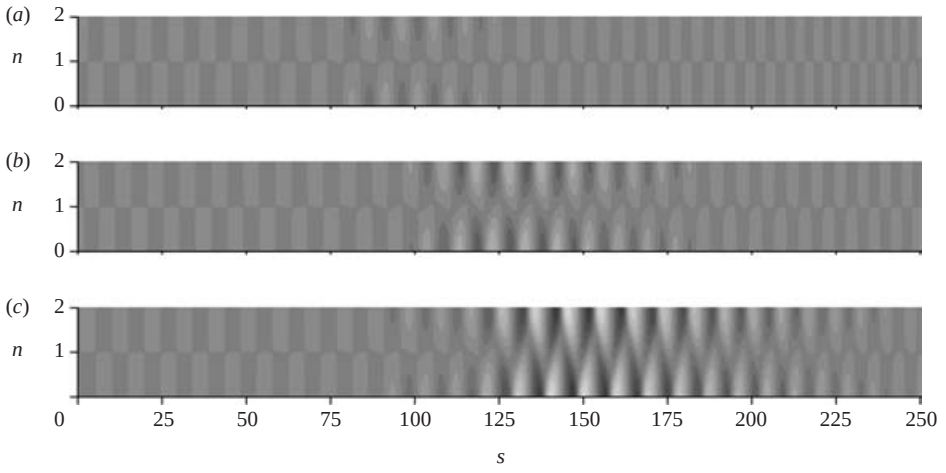

FIGURE 10. Bed topography generated by run '1Freq', performed by forcing a harmonic oscillation of bottom elevation at the initial cross-section. (*a*) $t = 2800$, (*b*) 3700 and (*c*) 4200 ($\tau_* = 0.057$, $d_s = 0.053$, $\beta = 8$ and $\beta_c = 5.6$).

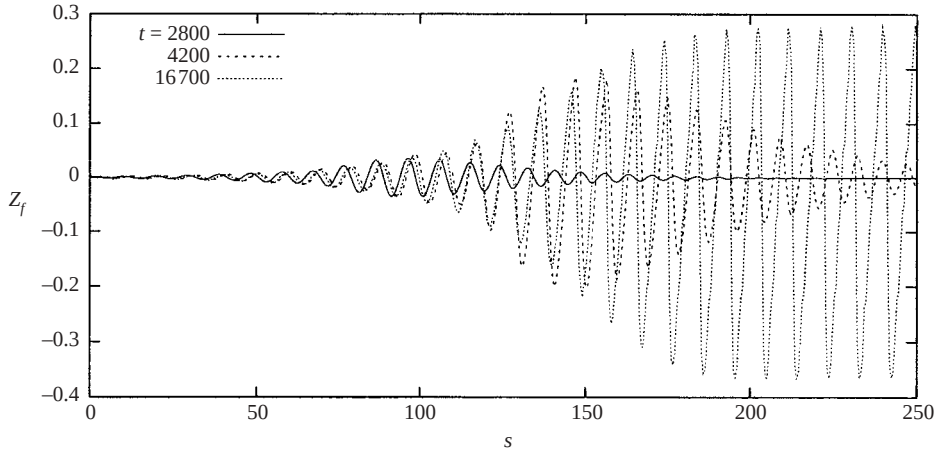

FIGURE 11. Distribution of bottom elevation along the right bank of the channel at different times in the run '1Freq'.

domain. The perturbation had a lateral distribution corresponding to the first alternate bar mode and oscillated periodically in time with a frequency chosen such that the corresponding wavenumber predicted by the dispersion relationship was characterized by the maximum temporal growth rate. The dimensionless amplitude of the initial perturbation (scaled by the average flow depth) was 10^{-3}. Figure 10 shows the results of the computation in the form of plots of bed topography corresponding to different times. The formation of a wave group is observed, which migrates downstream and undergoes spatial and temporal amplification keeping its tail in the upstream part of the domain.

Figure 11 shows the distribution of bottom elevation along the right bank in the same numerical experiment: note that nonlinear saturation occurs, hence the spatial–temporal amplification leads to the establishment of an equilibrium amplitude.

The equilibrium amplitude is found to be independent of the amplitude of the initial perturbation. This is shown in figure 12 where two different responses to

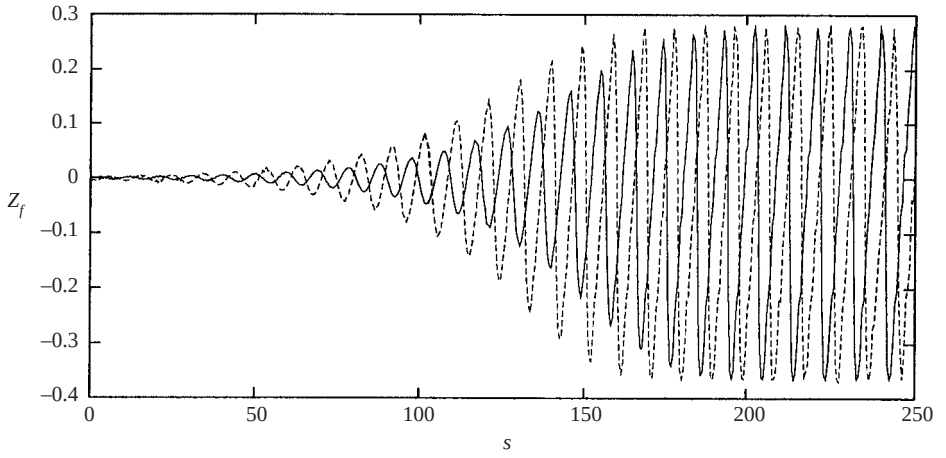

FIGURE 12. Comparison between the distributions of bottom elevation along the right bank of the channel in two experiments characterized by initial perturbations with equal frequency (the same as in run '1Freq') and different amplitudes. ——, dimensionless amplitude = 0.001; — — —, dimensionless amplitude = 0.002 ($\tau_* = 0.057$, $d_s = 0.053$, $\beta = 8$ and $\beta_c = 5.6$).

initial excitations identical except for their amplitudes (one twice the other) are reported. Note that the smaller the initial amplitude, the farther the cross-section where equilibrium is achieved.

We then attempted to ascertain whether a preferred mode selected by the spatial–temporal amplification of the initial perturbation could be detected. To this aim, we have forced an initial perturbation with the same lateral structure as before, but characterized by a temporal oscillation arising from the superposition of 20 harmonics of equal amplitudes and frequencies obtained from the dispersion relationship (run denoted '20Freq') having chosen 20 equally spaced unstable wavenumbers for the given value of the aspect ratio β (see figure 13). A more appropriate procedure would have been to impose a random oscillation; however, this leads to numerical instabilities due to the presence of frequencies that are too large in the forcing. We then repeated our calculation by halving the number of components of the forcing oscillation (run denoted '10Freq'). The harmonic content of the initial perturbation is not found to affect significantly either the equilibrium amplitude or the equilibrium wavenumber and wavespeed asymptotically reached by the perturbation. Figure 14 shows the temporal development of the bar wavenumber observed at different cross-sections during the run '20Freq'. Note that in the initial phase of the development process, the wavenumber most amplified exceeds one, whereas, approaching equilibrium the wavenumber evolves towards an asymptotic value of about 0.4. Such a value is slightly smaller than that corresponding to the maximum temporal growth rate of linear theory for the given aspect ratio of the channel. Similarly, figure 15 shows the temporal development of the bar celerity observed at different cross-sections during the run '20Freq'. Note that nonlinearity leads to a sharp decrease of the bar wavespeed in time. The latter results confirm the laboratory observations of Seminara & Tubino (1989*b*) and the calculations of Defina (2003).

6. Concluding remarks

The analysis developed in the present paper shows that the nature of bar instability is convective. Hence, as demonstrated through the numerical experiments discussed

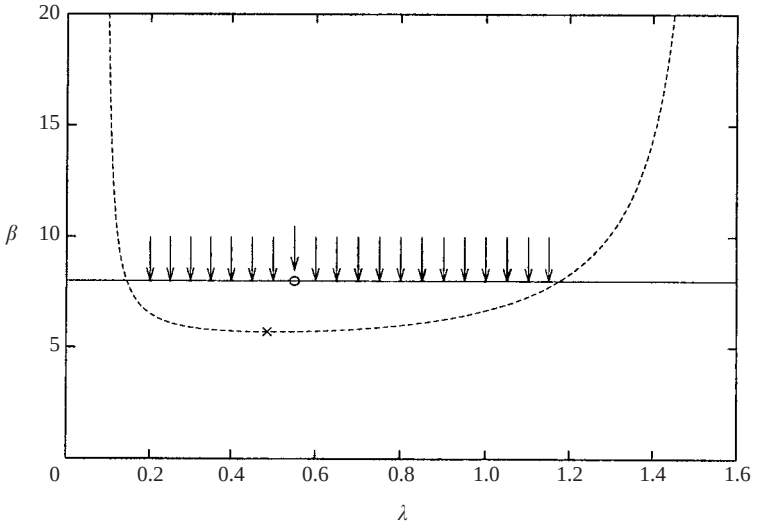

FIGURE 13. Sketch showing the 20 unstable wavenumbers such that the associated frequencies determined from the dispersion relationship contributed to the harmonic content of the initial perturbation of run '20Freq'. Note that the circle indicates the most unstable wavenumber for the given aspect ratio β according to the temporal linear stability theory, while the cross indicates the most unstable wavenumber at the marginal conditions. ($\tau_* = 0.057$, $d_s = 0.053$, $\beta = 8$ and $\beta_c = 5.6$).

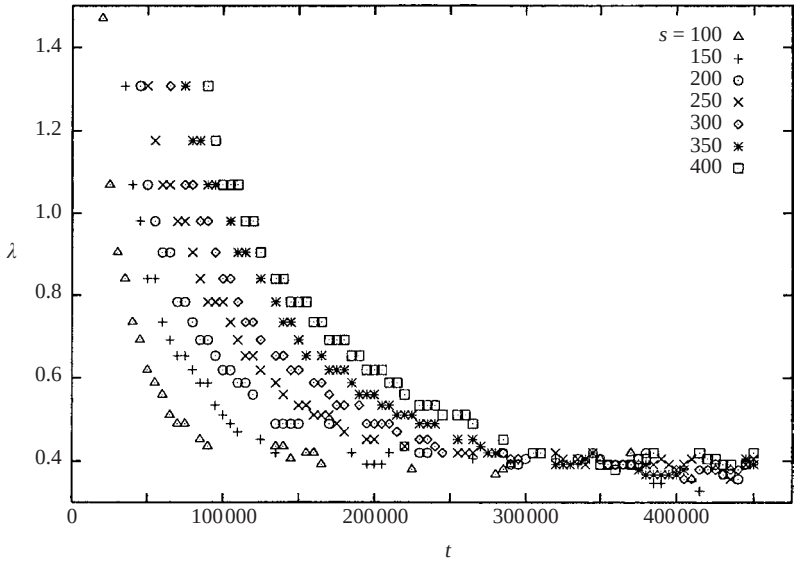

FIGURE 14. Temporal development of the bar wavenumber observed at different cross-sections in the run '20Freq' ($\tau_* = 0.057$, $d_s = 0.053$, $\beta = 8$ and $\beta_c = 5.6$).

in the previous section, the spatial–temporal development of bars arises from the persistent forcing of an initial perturbation. The structure of the finite-amplitude bars emerging from the nonlinear development exhibits a periodic pattern and an equilibrium amplitude, independent of the amplitude and harmonic content of the initial forcing. However, both the bar wavenumber and the bar speed do exhibit a temporal evolution whereby the perturbations lengthen and slow down as bar growth

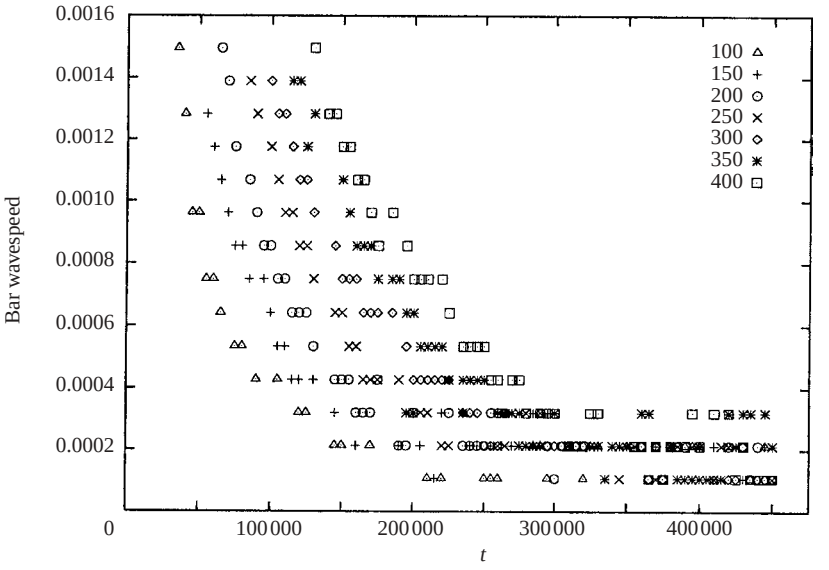

FIGURE 15. Temporal development of the bar celerity observed at different cross-sections in the run '20Freq' ($\tau_* = 0.057$, $d_s = 0.053$, $\beta = 8$ and $\beta_c = 5.6$).

moves from the linear into the nonlinear regime. Both such findings are in general agreement with the laboratory observations of Fujita & Muramoto (1985) (see also the analysis of Seminara & Tubino 1989*b*). However, the distance from the initial cross-section where equilibrium is achieved does depend on the intensity of the initial perturbation.

The latter finding raises important issues relating to the interpretation of laboratory observations of various authors (see Colombini *et al.* 1987, for references on experimental works). In fact, the question arises of whether the length of the experimental facility in the various experiments on bar formation was large enough to allow for the full development of perturbations. Indeed, the scatter of values of bar wavelength, bar speed and bar amplitude reported by different authors may be due partly to the exact location and time where the above features were observed. A detailed revisitation of such experimental works is then called for.

Needless to say, when moving from the laboratory to the field, the picture is considerably more complicated. The main additional feature introduced by the geometry of river channels is curvature. As mentioned in §1, a large body of knowledge has been developed in the last few decades about the hydrodynamic and morphodynamic effects of curvature in meandering rivers and it is well established that forced steady bars arise from the centrifugal and topographic secondary flows driven by curvature. The interaction of such forced features with the free perturbations arising from bar instability is known to give rise to a tendency for free bars to be suppressed when channel sinuosity is large enough (Kinoshita & Miwam 1974; Tubino & Seminara 1990). It is unlikely that the latter picture is significantly altered by the convective nature of free bars, though some strongly nonlinear calculations of the spatial–temporal development of free bars in sinuous channels would certainly be appropriate.

A second important feature brought up in the field is the presence of transport in suspension, when dealing with sandy rivers. Again, on purely intuitive grounds, we do not feel that the presence of a significant portion of sediments transported in

suspension should alter our conclusions about the convective nature of bar instability. However, such expectation can only be confirmed by a suitable extension of the present work to cover the effect of suspended load in the light of recent contributions (Repetto *et al.* 1999).

Further complicating features of the real world, such as grain sorting (Seminara 1995), unsteadiness (Tubino 1991) and geometrical constraints (Zolezzi & Seminara 2001) may also require additional attention in the light of the present results.

This work has been developed within the framework of the National Project cofunded by the Italian Ministry of University and of the Scientific and Technological Research and by the University of Genova (COFIN 2001) 'Morphodynamics of fluvial networks'. Partial support has also come from Fondazione Cassa di Risparmio di Verona, Vicenza, Belluno ed Ancona (Progetto RIMOF).

This work is also part of the PhD thesis of Bianca Federici to be submitted to the University of Padova in partial fulfilment of her degree.

The authors wish to thank Professor P. Hall for suggesting the importance of the problem and providing some useful references. The authors also wish to thank an anonymous referee for various suggestions which have contributed to improving the presentation of the paper.

REFERENCES

Bers, A. 1975 Linear waves and instabilities. *Physique des Plasmas* (ed. C. DeWitt & J. Peyraud), pp. 117–215. Gordon & Breach.

Bers, A. 1983 Space–time evolution of plasma instabilities – absolute and convective. *Handbook of Plasma Physics* (ed. M. N. Rosenbluth & R. Z. Sagdeev), vol. 1, pp. 451–517. North-Holland.

Briggs, R. J. 1964 *Electron-Stream Interaction with Plasmas*. MIT Press.

Blondeaux, P. & Seminara, G. 1985 An unified bar-bend theory of river meanders. *J. Fluid Mech.* **157**, 449–470.

Callander, R. A. 1969 Instability and river channels. *J. Fluid Mech.* **36**, 465–480.

Colombini, M., Seminara, G. & Tubino, M. 1987 Finite-amplitude alternate bars. *J. Fluid Mech.* **181**, 213–232 (referred to herein as CST).

Defina, A. 2003 Numerical experiments on bar growth. *Water Resour. Res.* **39**, art. no. 1092.

Engelund, F. & Skovgaard, O. 1973 On the origin of meandering and braiding in alluvial streams. *J. Fluid Mech.* **57**, 289–302.

Exner, F. M. 1925 Über die Wechselwirkung zwischen Wasser und geschiebe in Flüssen. *Sitzer Akad. Wiss. Wien* 165–180.

Federici, B. 1999 Experimental observations on bifurcations in braided rivers. Thesis, University of Genova. (In Italian.)

Federici, B. & Paola, C. 2003 Dynamics of bifurcations in noncohesive sediments. *Water Resour. Res.* (to appear).

Fujita, Y. & Muramoto, Y. 1985 Studies on the process of development of alternate bars. *Bull. Disaster Prevention Res. Inst.* **35**, 55–86.

Huerre, P. & Monkewitz, P. A. 1990 Local and global instabilities in spatially developing flows. *Annu. Rev. Fluid Mech.* **22**, 473–537.

Ikeda, S. & Parker, G. 1989 (Ed.) *River Meandering*. AGU Water Resources Monograph, vol. 12.

Ikeda, S., Parker, G. & Sawai, K. 1981 Bend theory of river meanders. Part 1. Linear development. *J. Fluid Mech.* **112**, 363–377.

Kinoshita, R. & Miwa, H. 1974 River channel formation which prevents downstream translation of transverse bars. *Shinsabo* **94**, 12–17. (In Japanese.)

Leopold, L. B. & Wolman, M. G. 1957. River channel patterns: braided, meandering and straight. *US Geol. Surv. Prof. Paper* **282-B**, 39–84.

Meyer-Peter, E. & Müller, R. 1948 Formulas for bedload transport. *III Conf. Intl Assoc. Hydraul. Res., Stockholm, Sweden.*

Parker, G. 1990 Surface-based bedload transport relation for gravel rivers. *J. Hydraul. Res.* **20**(4), 417–436.

Repetto, R., Tubino, M. & Zolezzi, G. 1999. Free bars in rivers. *J. Hydraul. Res.* **37**, 759–775.

Sekine, M. & Parker, G. 1992 Bed load transport on transverse slope – I. *J. Hydraul. Engng* ASCE, **118**, 513–535.

Seminara, G. 1995 Effect of grain sorting on the formation of bedforms. *Appl. Mech. Rev.* **48**, 549–563.

Seminara, G. & Tubino, M. 1989*a* Alternate bars and meandering: free, forced and mixed interactions. In *River Meandering* (ed. S. Ikeda & G. Parker), AGU Water Resources Monograph, vol. 12, pp. 267–320.

Seminara, G. & Tubino, M. 1989*b* On the process of meander formation. *IV Intl Symp. River Sedimentation, Beijing, China*, pp. 873–880.

Seminara, G. & Tubino, M. 2001 Sand bars in tidal channels. Part 1. Free bars. *J. Fluid Mech.* **440**, 49–74.

Shields, A. 1936 Anwendung der Ähnlichkeitsmechanik und der Turbulenzforschung auf die Geschiebebewegung. *Mitt. Preuss. Versuchsanst. Wasserbau Schiffbau*, vol. 26.

Talmon, A. M., Struiksma, N. & Van Mierlo, M. C. L. M. 1995 Laboratory measurements of the sediment transport on transverse alluvial-bed slopes. *J. Hydraul. Res.* **33**, 519–534.

Tubino, M. 1991 Growth of alternate bars in unsteady flow. *Water Resour. Res.* **27**, 37–52.

Tubino, M. & Seminara, G. 1990 Free-forced interactions in developing meanders and suppression of free bars. *J. Fluid Mech.* **214**, 131–159.

Zolezzi, G. & Seminara, G. 2001 Downstream and upstream influence in river meandering. Part 1. General theory and application to overdeepening. *J. Fluid Mech.* **438**, 183–211.